ACS OMEGA

Open Access

http://pubs.acs.org/journal/acsodf

Article

A Novel 3-*meta*-Pyridine-1,2,4-oxadiazole Derivative of Glycyrrhetinic Acid as a Safe and Promising Candidate for Overcoming P-Glycoprotein-Mediated Multidrug Resistance in Tumor Cells

Arseny D. Moralev, Oksana V. Salomatina, Ivan V. Chernikov, Nariman F. Salakhutdinov, Marina A. Zenkova, and Andrey V. Markov*

Cite This: *ACS Omega* 2023, 8, 48813−48824

Read Online

ACCESS | Metrics & More | Article Recommendations | Supporting Information

ABSTRACT: Given the pharmacophore properties of the nitrogen-containing moiety in the molecular structure of P-glycoprotein (P-gp) inhibitors, we report the evaluation of the P-gp inhibitory and MDR reversal activities of **2g**, a 3-*meta*-pyridin-1,2,4-oxadiazole derivative of 18β*H*-glycyrrhetinic acid. Through molecular docking, we have shown that **2g** has the potential to directly interact with the transmembrane domain of P-gp with a low free binding energy (−10.2 kcal/mol). Using KB-8-5 human cervical carcinoma cells and RLS40 murine lymphosarcoma cells, both of which exhibit a multidrug-resistant (MDR) phenotype mediated by P-gp activation, we have shown that **2g**, at nontoxic concentrations, effectively increased the intracellular accumulation of fluorescent P-gp substrates (rhodamine 123 or doxorubicin (DOX)), leading to a marked sensitization of the model cells to the cytotoxic effect of DOX. Considering the comparable activity of **2g** with verapamil, a known P-gp inhibitor, **2g** can be considered as a promising candidate for the development of agents capable of overcoming P-gp-mediated MDR in tumor cells.

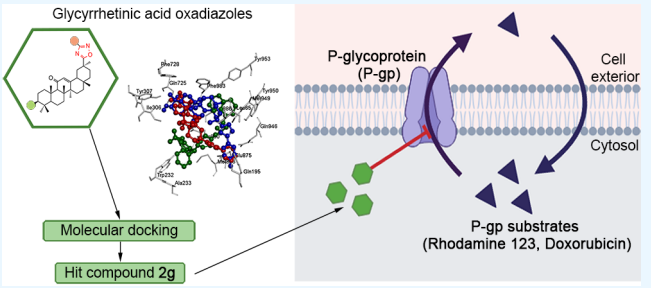

INTRODUCTION

Despite recent advances in understanding the factors underlying the development of multidrug resistance (MDR), this process remains one of the current challenges in cancer treatment.[1] The key MDR-inducing mechanism is associated with the hyperexpression of transmembrane drug transporters from the ATP-binding cassette (ABC) family, which promote the transport of xenobiotics across cell membranes.[2] The most studied ABC efflux transporter is P-glycoprotein (P-gp), which is constitutively expressed in various tissues and tumor cells acquiring the MDR phenotype.[3,4] P-gp exhibits broad substrate specificity for a number of hydrophobic compounds, including clinically important antineoplastic drugs.[5,6] Given the crucial role of P-gp in reducing the chemosensitivity of tumor cells, the development of P-gp inhibitors is considered as a promising strategy for antitumor therapy.[6,7] Three generations of P-gp inhibitors are currently known; however, to the best of our knowledge, none of them have been approved for clinical use. Although some third-generation P-gp inhibitors, such as zosuquidar, elacridar, and tariquidar, have reached clinical trials, the results obtained in most cases were unsatisfactory due to undesirable side effects and toxicity.[8] Thus, new strategies are needed to develop effective P-gp inhibitors to overcome MDR.

Despite the proven efficacy of synthetic chemicals as efflux transporter blockers, the use of natural metabolites in the development of P-gp inhibitors is still appreciated due to their low systemic toxicity, multitarget effects, and structural diversity.[9−11] Given that nitrogen-containing cyclic moieties are considered a privileged pharmacophore for ABC transporter inhibitors,[7,12,13] a variety of phytochemical derivatives with similar functionality (Figure 1) have been developed as promising P-gp inhibitors, which effectively reverse MDR in tumor cells both *in vitro* and *in vivo*.[14−18] Interestingly, pentacyclic triterpenoids are known to exhibit a significant synergistic effect with various anticancer drugs.[19−21] However, to our knowledge, there are only a few reports regarding their suppressive effect on P-gp activity,[14,18,20,22] and none of these studies have specifically examined the P-gp inhibitory potency of triterpenoids bearing N-containing cyclic substituents.

Received: August 21, 2023
Revised: December 4, 2023
Accepted: December 6, 2023
Published: December 12, 2023

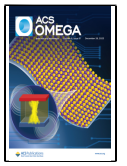

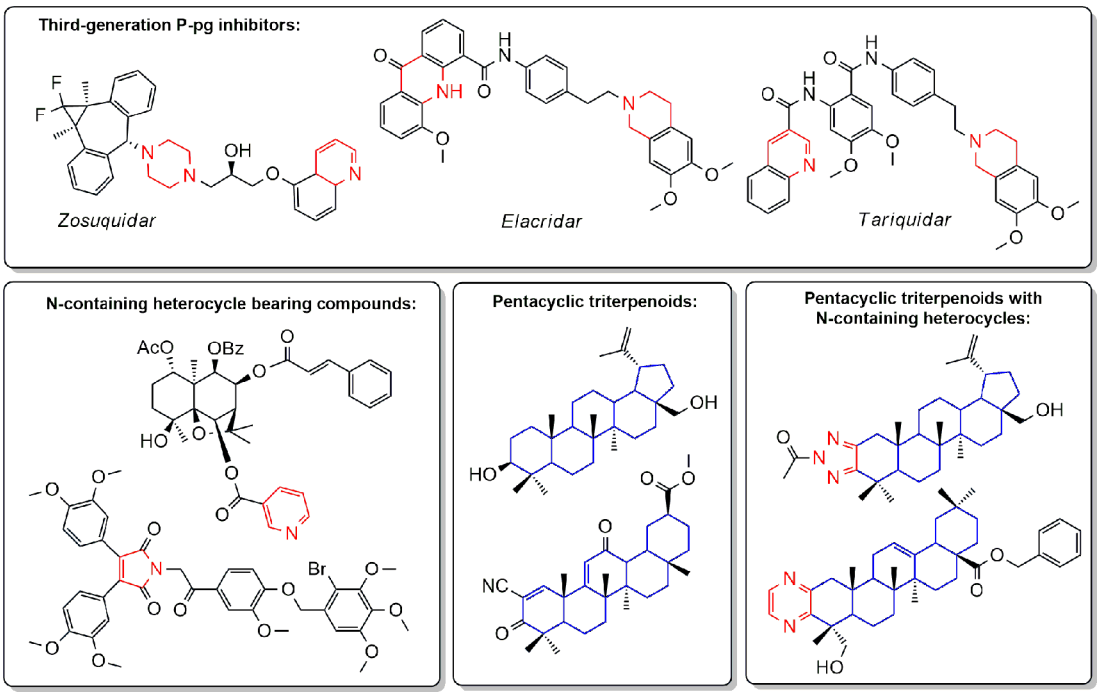

Figure 1. Structures of third-generation P-gp inhibitors and semisynthetic derivatives of natural compounds bearing N-containing heterocycles and pentacyclic triterpenoid backbones that display promising P-gp inhibitory activity. N-containing heterocyclic groups and triterpenoid scaffolds are marked with red and blue colors, respectively.

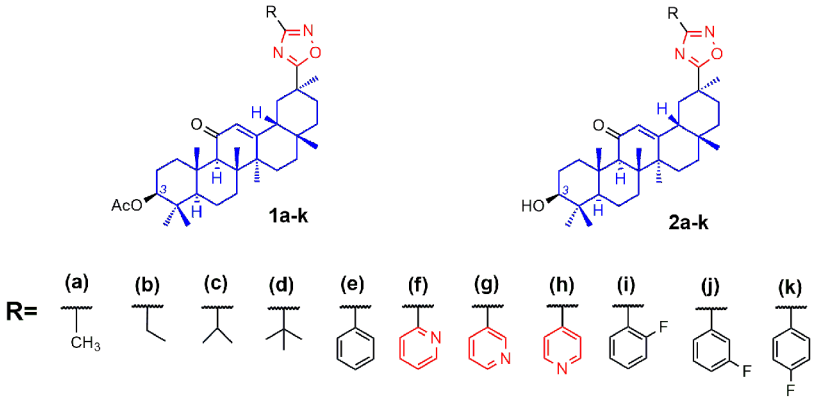

Figure 2. Structure of GA derivatives **1a−k** and **2a−k**. Blue-colored and red-colored structures represent a pentacyclic triterpenoid scaffold and nitrogen-containing heterocycles, respectively.

Thus, the present study aimed to answer the question of whether pentacyclic triterpenoids modified with nitrogen-containing functional groups are capable of blocking the efflux activity of P-gp and reversing the MDR phenotype in tumor cells. To address this issue, we focused on semisynthetic derivatives of 18βH-glycyrrhetinic acid (GA) obtained by transforming its native carboxyl group into a 1,2,4-oxadiazole fragment bearing different moieties at C-3, including aliphatic (**1a−d**, **2a−d**), phenyl (**1e−2e**), and pyridine (**1f−h**, **2f−h**) groups (Figure 2). Additionally, considering that fluorination has great potential to enhance drug efficacy[23] and the presence of fluorine groups in the zosuquidar structure (Figure 1), GA derivatives containing fluorine-substituted phenyl rings (**1i−k**, **2i−k**) were included in the study (Figure 2). Using molecular modeling, the interaction of GA derivatives with the active site of P-gp was explored, and the MDR reversal activity of the selected hit compound was thoroughly verified, providing new insights for further progress in the development of novel P-gp inhibitors.

2. RESULTS AND DISCUSSION

2.1. 1A−F AND 2A−F CAN BIND TO THE SUBSTRATE-BINDING DOMAIN OF P-GP

First, to assess the P-gp suppressive potential of GA derivatives, their substrate and inhibitor activities for P-gp were predicted using three independent chemoinformatics web tools, namely ADMETlab,[24] SwissADME,[25] and LiverTox.[26] To ensure the reliability of the prediction, doxorubicin (DOX) and verapamil (VPM), the well-known substrate[27] and inhibitor[35] of P-pg, respectively, were included in the analysis. As depicted in Figure 3A, the chemoinformatics platforms adequately predicted DOX and VPM as P-gp-specific substrates and inhibitors, respectively, and showed a low susceptibility of all

https://doi.org/10.1021/acsomega.3c06202
ACS Omega 2023, 8, 48813−48824

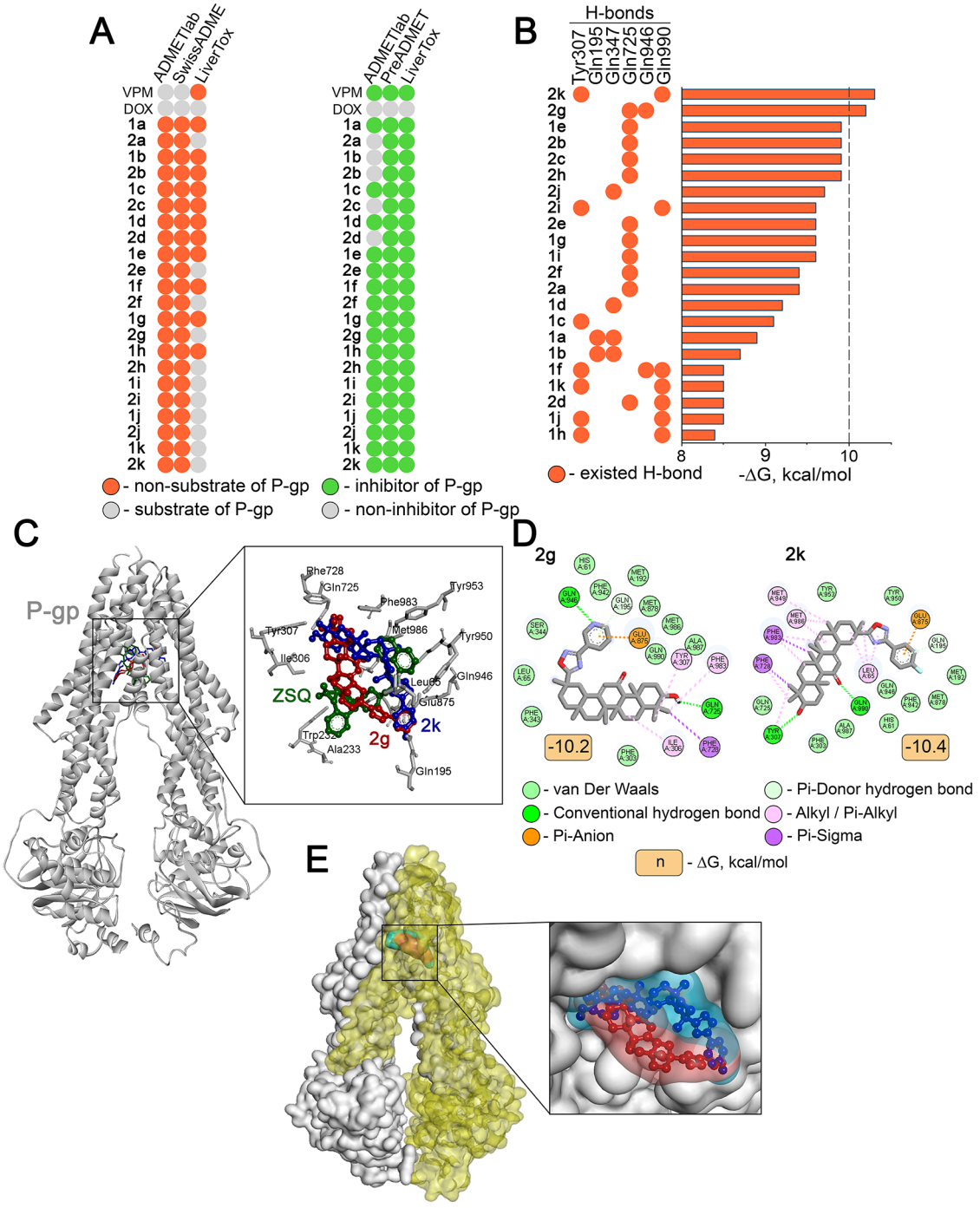

Figure 3. Ability of 3-substituted 1,2,4-oxadiazoles of GA to bind to the transmembrane domain of P-gp. (A) *In silico* prediction of substrate specificity for P-gp and P-gp inhibitory potential of GA derivatives. (B) Binding energies and hydrogen bonds formed by compounds **1a**−**h** and **2a**−**h** with the transmembrane domain of P-gp. Molecular docking was performed by using AutoDock Vina. (C) Three-dimensional representation of the molecular interaction of zosuquidar (ZSQ), **2g**, and **2k**, and in the transmembrane domain of P-gp. Green-, red-, and blue-colored molecules represent ZSQ, **2g**, and **2k**, respectively. (D) Two-dimensional representation of the molecular interaction between **2g** or **2k** and the transmembrane domain of P-gp. (E) Surface diagram of the docked **2g** and **2k** shown in the central cavity of the transmembrane domain of P-gp. Red- and blue-colored surfaces represent **2g** and **2k**, respectively.

tested GA derivatives to P-gp efflux transport and their probable suppressive effect on P-gp activity.

Next, to verify the obtained data, the binding interactions of GA derivatives with P-gp were evaluated by using a molecular docking approach. The performed analysis showed that all explored triterpenoids could interact with the transmembrane domain of the transporter with a low binding energy (ΔG) ranging from −8.4 to −10.4 kcal/mol (Figure 3B,C). Moreover, the majority of the tested molecules (15 out of 22) exhibited a strong affinity with P-gp ($\Delta G < -9$ kcal/mol) (Figure 3B). Based on the obtained molecular simulation results, the following remarks can be made:

- the C-3 hydroxyl group in the triterpenoid scaffold (**2a**−**k**) is more favorable than the C-3 acetoxy group (**1a**−**k**)

https://doi.org/10.1021/acsomega.3c06202
ACS Omega 2023, 8, 48813−48824

Scheme 1. Synthesis of Compounds 1g, 1k, 2g, and 2k and Intermediates 4g and 4k[a]

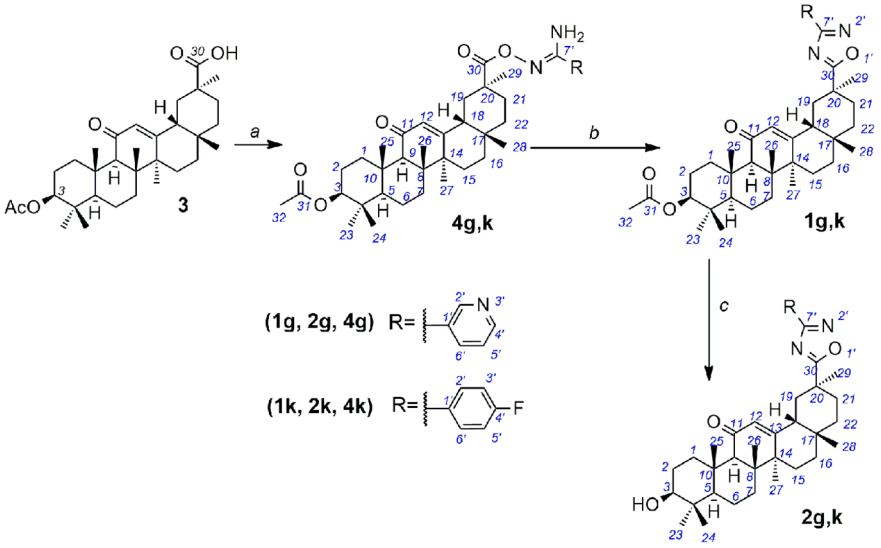

[a]Reagents and conditions: (a) *N*,*N*′-carbonyldiimidazole (CDI), CH_2Cl_2, room temperature (RT), 2 h; then *N*′-hydroxynicotinimidamide (for **1g**) or 4-fluoro-*N*′-hydroxybenzimidamide (for **1k**), RT, overnight. (b) TBA−OH, CH_2Cl_2−MeOH, RT, 1−2 h; (c) KOH, *i*-PrOH−H_2O, RT overnight.

since compounds **2a−k** formed more stable complexes with P-gp compared to **1a−k** (average ΔG^{2a-k} = −9.7 kcal/mol vs average ΔG^{1a-k} = −8.9 kcal/mol);

- 1,2,4-Oxadiazole group does not participate in the formation of hydrogen bonds with P-gp and, therefore, can be only considered as a linker that properly connects the triterpenoid scaffold with various anti-P-gp-relevant functional groups;
- *meta*-Pyridine substituent at C-3 in the 1,2,4-oxadiazole ring (**1g** and **2g**) is a more preferred group compared to isomeric *ortho*-pyridine (**1f** and **2f**) and *para*-pyridine (**1h** and **2h**) (ΔG^{1g} = −9.6 kcal/mol vs ΔG^{1f} = −8.5 kcal/mol and ΔG^{1h} = −8.4 kcal/mol; ΔG^{2g} = −10.2 kcal/mol vs ΔG^{2f} = −9.4 kcal/mol and ΔG^{2h} = −9.9 kcal/mol);
- fluorination of the phenyl substituent does not generally increase the binding affinity of phenyl-bearing GA derivatives to P-gp, with the exception of compound **2k**, which contains a *para*-fluorophenyl moiety (ΔG^{1e} = −9.9 kcal/mol vs average ΔG^{1i-k} = −8.9 kcal/mol; ΔG^{2e} = −9.6 kcal/mol vs average $\Delta G^{2i,j}$ = −9.6 kcal/mol).

Two derivatives of 1,2,4-oxadiazole GA demonstrating the lowest binding energies were chosen as hit compounds, namely, **2g** and **2k**, with a *meta*-pyridine and *para*-fluorophenyl substituent at C-3, respectively. As shown in Figure 3D, **2g** and **2k** formed hydrogen bonds with Gln725 and Gln946 as well as Tyr307 and Gln990, respectively (Figure 3D), which play an important role in the ATP hydrolytic activity of P-gp.[28−31] These findings, along with the observed high surface complementarity between the tested molecules and P-gp (Figure 3E), confirmed the P-gp-inhibitory potential of the hit compounds, which requires experimental confirmation.

2.2. SYNTHESIS OF THE HIT COMPOUNDS 2G AND 2K

The hit compounds **2g** and **2k** were obtained by converting the natural carboxyl group of GA into a 1,2,4-oxadiazole ring according to the following strategy: (1) acylation of the corresponding *N*′-hydroxyimidamide with the activated carboxylic group of starting triterpenoid; (2) cyclization of *O*-acylated amidoximes.

3-Acetoxy-18β*H*-glycyrrhetinic acid (**3**), a product of acetic acid hydrolysis of glycyrrhizin, was used as the starting material for the synthesis (Scheme 1). Compound **2g** was obtained previously,[34] but here we modified the step of oxadiazole ring formation by replacing the cyclizing agent tetra-*n*-butylammonium fluoride (TBAF) with tetra-*n*-butylammonium hydroxide (TBA−OH). This modification allowed us to slightly increase the yield of the product (from 75% to 87%) and eliminate one water treatment.

The synthesis of compounds **2g** and **2k** is shown in Scheme 1. First, 4-fluoro-*N*′-hydroxybenzimidamide and *N*′-hydroxynicotinimidamide were obtained from the corresponding nitrile and hydroxylamine according to the published procedure.[32] Activation of the carboxyl group of triterpenoid derivative **3** with *N*,*N*′-carbonyldiimidazole (CDI) and subsequent reaction with the corresponding *N*′-hydroxyimidamide afforded intermediates **4g** and **4k** in 94% and 87% yields, respectively. Next, the 1,2,4-oxadiazole ring was formed by treating intermediates **4g** and **4k** with catalytic amounts of TBA−OH in CH_2Cl_2−MeOH; derivatives **1g** and **1k** were obtained in yields of 87% and 79% after purification by flash chromatography, respectively. Finally, alkaline hydrolysis of the 3-acetoxy group in the triterpenoid scaffold led to the formation of target compounds **2g** and **2k** with yields of 78% and 80%, respectivley.

The final products were obtained in a total yield of 64% for **2g** and 55% for **2k**. The reagents required for the synthesis are cheap and commercially available; all reactions proceed with the formation of predominantly one product, which can be used in subsequent stages without purification.

https://doi.org/10.1021/acsomega.3c06202
ACS Omega 2023, 8, 48813−48824

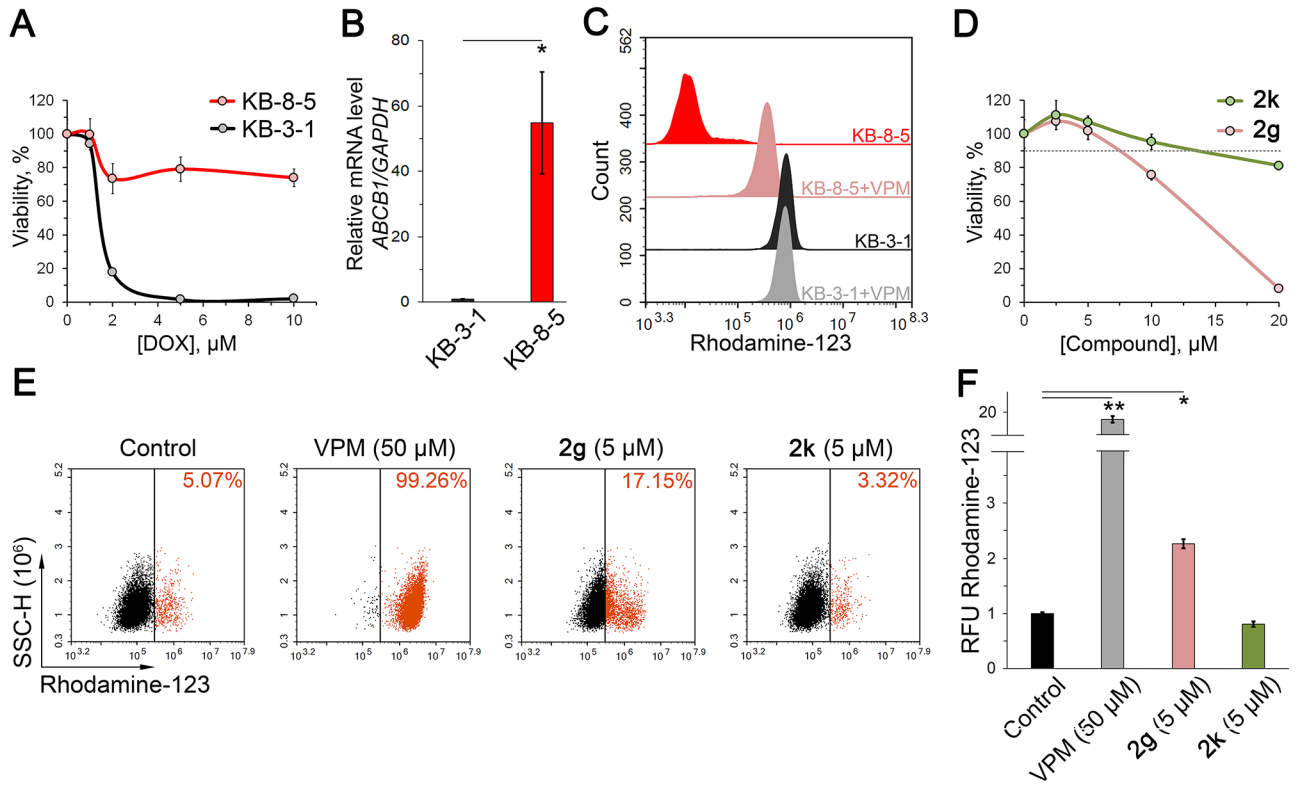

Figure 4. Effects of **2g** and **2k** on Rhodamine-123 (Rho123) uptake by KB-8-5 cells. (A) The sensitivity of KB-3-1 and KB-8-5 cells to DOX (1−10 μM) evaluated by the MTT test after 72 h of incubation. (B) Relative mRNA levels of ABCB1/GAPDH in KB-3-1 and KB-8-5 cells assessed using qRT-PCR. (C) Rho123 fluorescence intensity in KB-3-1 and KB-8-5 cells after exposure to VPM (50 μM) and Rho123 (5.25 μM) for 30 min. (D) The cytotoxicity of **2g** and **2k** in KB-8-5 cells assessed using the MTT test for 72 h. (E) Representative flow cytometry dot plots of Rho123 fluorescence versus SSC-H of KB-8-5 cells treated with Rho123, VPM, **2g**, and **2k** for 30 min. Control − untreated cells incubated with Rho123 only. (F) Relative fluorescence intensity of KB-8-5 cells incubated with Rho123, VPM, **2g**, and **2k**. Control − untreated cells incubated with Rho123. *$p < 0.05$; **$p < 0.01$.

2.3. 2G ENHANCED THE ACCUMULATION OF RHODAMINE 123 IN KB-8-5 CELLS WITH MDR PHENOTYPE

To verify our molecular modeling results, the MDR reversal activity of hit compounds was explored in human cervical carcinoma KB-8-5 cells with the MDR phenotype.[33] First, to ensure the MDR status of KB-8-5 cells, a range of their MDR-related traits were evaluated. Indeed, compared to parental MDR-negative human cervical carcinoma KB-3-1 cells,[34] KB-8-5 cells were found to exhibit significantly lower susceptibility to DOX (Figure 4A) and 54.8-fold upregulation of *ABCB1* encoding P-gp (Figure 4B). Moreover, KB-8-5 cells were characterized by low intracellular accumulation of Rhodamine 123 (Rho123), a known fluorescent P-gp substrate,[35] while VPM treatment significantly increased this parameter nearly to the level of MDR-negative KB-3-1 cells (Figure 4C). Thus, a performed analysis clearly indicated the applicability of KB-8-5 cells as a relevant model to explore the anti-P-gp activity of hit compounds.

Next, a nontoxic concentration of **2g** and **2k** at 5 μM was identified using the MTT assay (Figure 4D). Subsequently, the effect of selected triterpenoids on Rho123 accumulation in KB-8-5 cells was assessed. It was found that treating the cells with **2g** increased the percentage of Rho123-positive cells by 3.4-fold (Figure 4E) and enhanced intracellular Rho123 accumulation by 2.3-fold (Figure 4F) compared to that of the control. Surprisingly, **2k** showed no obvious impact on Rho123 accumulation (Figure 4E,F), which can be explained by the peculiarities of the interaction between **2k** and P-gp upon binding. It has been known that Gln725 is a residue crucial for the binding of known inhibitors of P-gp, including tariquidar, valinomycin, and cyclosporine A, since its mutation leads to complete loss of the ability of these compounds to inhibit transport activity of P-gp.[36] Although **2k** can interact with multiple active site residues, hydrogen bond interactions with Gln725 were missing in the complex of **2k** with P-gp. Moreover, the presence of *meta*-pyridine in **2g** results in hydrogen bond formation with Gln946, which allows **2g** to occupy a position more close to the zosuquidar position compared to **2k** (Figure 3C,D). We hypothesize that this arrangement of **2g** more efficiently prevents the conformational shift of transmembrane helix 9 of P-gp, which is crucial for initiating pump activity of P-gp.[37] However, further molecular dynamics studies are needed to confirm this hypothesis. Despite the observed less pronounced inhibitory potential of **2g** on P-gp efflux activity compared to VPM (Figure 4E,F), **2g** exhibited a statistically significant effect at a 10-fold lower concentration than VPM, which indicates the expediency of its further investigation as a P-gp inhibitor candidate. This is also supported by the low level of toxicity of **2g** demonstrated previously against nontransformed human hFF3 fibroblasts ($IC^{(48\ h)}_{50}$ > 50 μM)[38] and in the present study against nonmalignant human embryonic kidney HEK293 cells ($IC^{(72\ h)}_{50}$ significantly greater than 20 μM) (Figure S1).

https://doi.org/10.1021/acsomega.3c06202
ACS Omega 2023, 8, 48813−48824

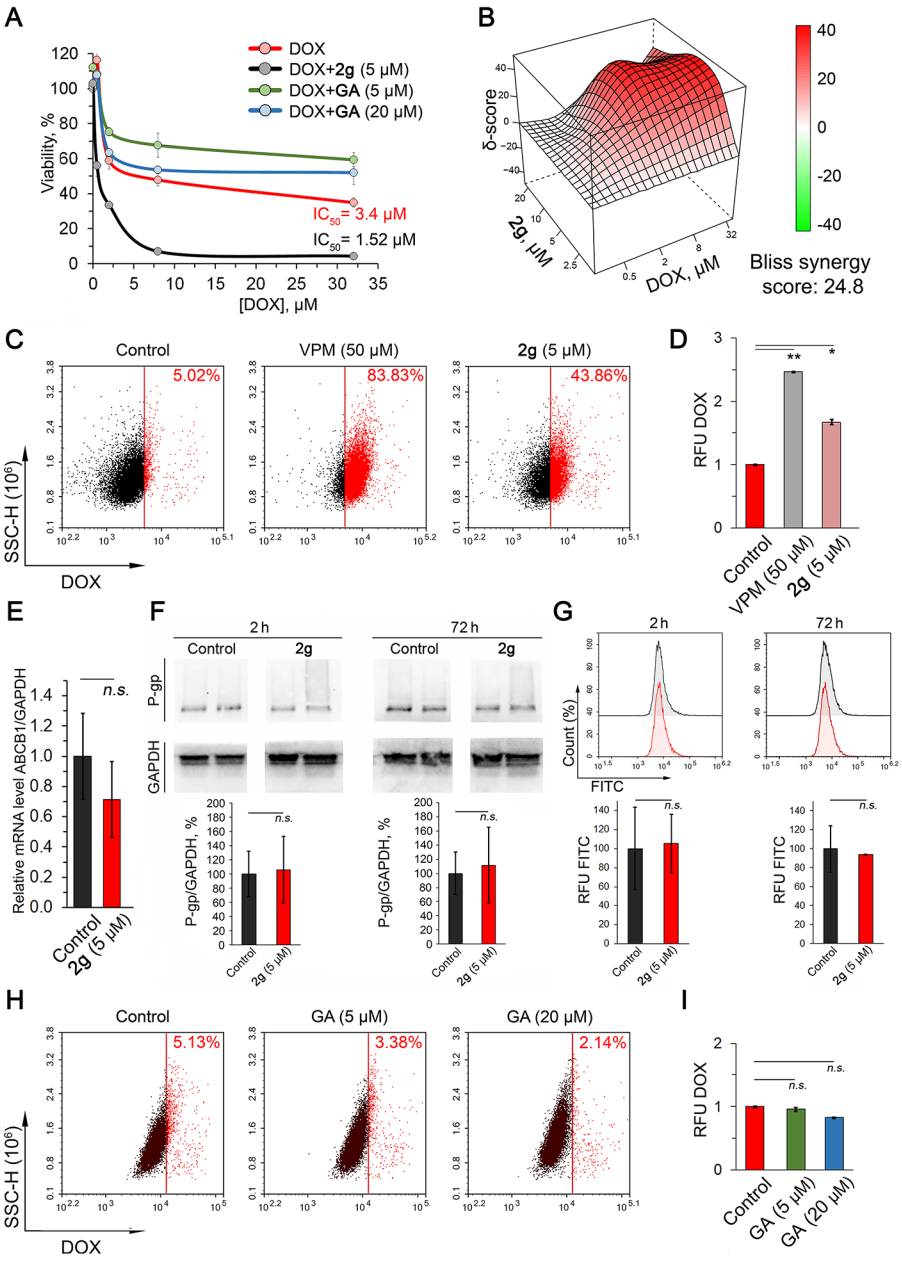

Figure 5. Effects of **2g** and **GA** on doxorubicin (DOX) uptake and MDR reverse in KB-8-5 cells. (A) The effect of **2g** and **GA** on the cytotoxicity of DOX in KB-8-5 cells. KB-8-5 cells were incubated with doxorubicin (0.5−32 μM) in the presence or absence of **2g** (5 μM) or **GA** (5 or 20 μM) for 72 h, followed by the assessment of cell viability using the MTT assay. (B) Synergy plot of DOX and **2g**-treated KB-8-5 cells. The Bliss synergy score was calculated and plotted using the SynergyFinder tool.[40] (C) Representative flow cytometry dot plots of DOX fluorescence versus SSC-H of KB-8-5 cells treated with DOX, VPM, and **2g** for 2 h. Control refers to untreated cells incubated with DOX only. (D) Relative fluorescence intensity of KB-8-5 cells incubated with DOX, VPM, and **2g**. Control refers to untreated cells incubated with DOX only. (E) Relative mRNA level of ABCB1/GAPDH in KB-8-5 cells after incubation with **2g** for 72 h evaluated by qRT-PCR. Control − untreated cells. (F) Western blot analysis of P-glycoprotein levels in KB-8-5 cells treated with **2g** (5 μM) for 2 and 72 h. Control − untreated cells. (G) Expression of P-gp in KB-8-5 cells treated with **2g** (5 μM) for 2 and 72 h assessed by flow cytometry. (H) Representative flow cytometry dot plots of DOX fluorescence versus SSC-H of KB-8-5 cells incubated with DOX and **GA** for 2 h. Control refers to untreated cells incubated with DOX only. (I) Relative fluorescence intensity of KB-8-5 cells incubated with DOX and **GA**. Control refers to untreated cells incubated with DOX only. Data are presented as the mean ± SD. *p < 0.05; **p < 0.01, *n.s.* − not significant.

2.4. 2G ENHANCED TOXICITY AND INTRACELLULAR ACCUMULATION OF DOX IN KB-8-5 CELLS

Given the demonstrated ability of **2g** to inhibit the P-gp-mediated efflux of Rho123, its potential to reverse DOX resistance in KB-8-5 cells was further investigated. As shown in Figure 5A, **2g** at 5 μM 2.3-fold enhanced the susceptibility of KB-8-5 cells to DOX cytotoxicity. In accordance with these results, the combination of **2g** with DOX demonstrated strong synergism in the Bliss model, with a synergy score of 24.8 (Figure 5B). To determine whether the observed effects of **2g** are associated with its inhibitory effect on DOX efflux, flow cytometry analysis was performed. It was found that the cotreatment of KB-8-5 cells with DOX and **2g** indeed 8-fold increased the population of DOX-positive cells (Figure 5C)

https://doi.org/10.1021/acsomega.3c06202
ACS Omega 2023, 8, 48813−48824

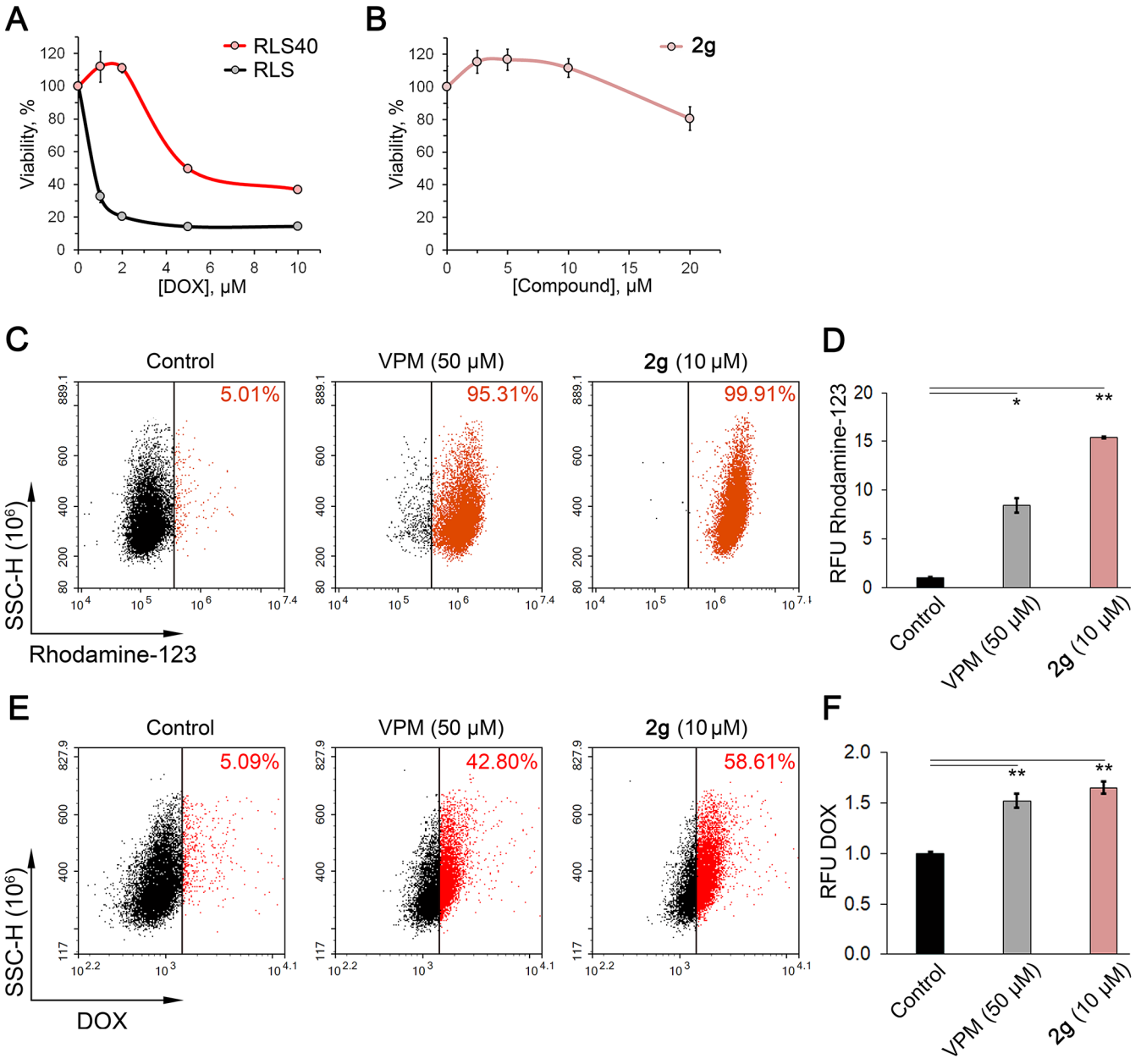

Figure 6. Verification of P-gp inhibitory activity of **2g** in murine lymphosarcoma RLS40 cells. (A) The sensitivity of RLS and RLS40 cells to DOX (0.5−32 μM) evaluated by the WST test after 72 h of incubation. (B) The cytotoxicity of **2g** in RLS40 cells evaluated by the WST test after 72 h of incubation. (C) Representative flow cytometry dot plots of Rho123 fluorescence versus SSC-H of RLS40 cells treated with Rho123, VPM, and **2g** for 2 h. Control refers to untreated cells incubated with Rho123 only. (D) The accumulation of Rho123 in RLS40 cells treated with VPM or **2g**. Control refers to untreated cells incubated with Rho123 only. (E) Representative flow cytometry dot plots of DOX fluorescence versus SSC-H of RLS40 cells treated with DOX, VPM, and **2g** for 2 h. Control refers to untreated cells incubated with DOX only. (F) Relative fluorescence intensity of RLS40 cells incubated with DOX, VPM, and **2g**. Control refers to untreated cells incubated with DOX only. *$p < 0.05$; **$p < 0.01$.

and 1.7-fold enhanced intracellular DOX uptake (Figure 5D) compared to the control, demonstrating a similar effect with VPM, albeit less pronounced. Interestingly, the effect of VPM on Rho123 uptake (Figure 4E,F) was more pronounced compared to DOX uptake (Figure 5C,D), which can be explained by the differences in the binding sites of Rho123 and DOX in P-gp that impact VPM efficacy.[39] Performed RT-PCR, Western blot, and flow cytometry analysis revealed no statistically significant changes in both ABCB1 mRNA and protein levels in KB-8-5 cells in response to **2g** (Figures 5E−G and S2) that independently confirmed the direct inhibitory effect of **2g** on P-gp activity. Notably, GA, the parental compound of **2g**, at similar concentrations (5 and 20 μM) did not enhance the cytotoxicity of DOX (Figure 5A) and its intracellular accumulation in KB-8-5 cells (Figure 5H,I), which provides useful information for structure−activity relationship-based optimization of candidate P-gp polycyclic inhibitors.

2.5. 2G EXHIBITS PRONOUNCED MDR REVERSAL EFFECT IN RLS40 CELLS

Given the ability of well-known P-gp inhibitors to suppress the MDR phenotype of tumor cells regardless of their origins and species,[41] we next questioned whether **2g** inhibits the efflux of P-gp substrates from murine RLS40 lymphosarcoma cells

https://doi.org/10.1021/acsomega.3c06202
ACS Omega 2023, 8, 48813−48824

overexpressing P-gp.[42] First, we verified the lower susceptibility of RLS40 cells to DOX compared with the parental RLS cell line (Figure 6A) and identified a nontoxic concentration of **2g** at 10 μM for further analysis (Figure 6B).

It was found that **2g** significantly suppressed the transport activity of P-gp in RLS40 cells, demonstrating efficacy comparable to or even superior to that of VPM (Figure 6C−F). The treatment of RLS40 cells with **2g** increased the population of Rho123-positive cells to 99.9% and enhanced intracellular Rho123 uptake by 15.4-fold compared to that of the control (Figure 6C,D). In the case of DOX-treated RLS40 cells, **2g** also increased the percentage of DOX-positive cells and the level of relative DOX fluorescence intensity in the cells by 11.5 (Figure 6E) and 1.5 times (Figure 6F) compared with the control, respectively. The more pronounced susceptibility of RLS40 cells to **2g** compared with KB-8-5 cells can be explained by the dose-dependent effect of the studied compound (working concentrations of **2g** at 10 and 5 μM in RLS40 and KB-8-5 cells, respectively). Thus, the obtained results independently confirmed the MDR reversal activity of **2g** and suggested that pentacyclic triterpenoids bearing N-containing heterocycles can be considered as a promising platform to develop novel P-gp inhibitors.

3. CONCLUSION

To summarize, the molecular docking screening of GA derivatives containing 3-substituted-1,2,4-oxadiazole moieties revealed that attaching the *meta*-pyridine moiety via a 1,2,4-oxadiazole linker at the C-20 position of GA markedly enhanced the binding affinity of explored semisynthetic triterpenoids to the transmembrane domain of P-gp. The revealed hit compound **2g** exhibited a low free binding energy and formed hydrogen bonds with amino acid residues that play a critical role in the P-gp efflux activity. Further *in vitro* studies confirmed the promising potential of the hit compound as a P-gp inhibitor. It was found that **2g** effectively suppressed the P-gp-mediated efflux of Rho123 and DOX from human multidrug-resistant KB-8-5 cells, thereby sensitizing them to the cytotoxic effects of DOX in a synergistic manner. The obtained results were additionally verified in RLS40 cells with the MDR phenotype, where **2g** effectively increased the intracellular uptake of Rho123 and DOX with efficacy compared with that of VPM. Obtained results provide valuable information about the structure−activity relationship of N-heterocyclic-bearing triterpenoids and highlight the potential of pyridine-bearing compounds as promising scaffolds for designing P-gp inhibitors. Given that P-gp is overexpressed at the apical side of many barriers mediating the efflux of xenobiotic compounds from the intestine, liver, kidney, blood−brain barrier, and placenta,[43] the revealed synergistic cytotoxic effect of **2g** and DOX suggests the necessity for further investigation into the toxic profile of **2g** when combined with other pharmacologically active compounds in animal models.

4. MATERIALS AND METHODS

4.1. CHEMISTRY

4-Fluorobenzonitrile, nicotinonitrile, and CDI were purchased from ACROS Organics. Tetra-*n*-butylammonium hydroxide (TBA−OH) 1.0 M solution in methanol was purchased from Alfa Aesar. All solvents required for the synthesis were purified and dried according to standard procedures. 4-Fluoro-*N*′-hydroxybenzimidamide and *N*′-hydroxynicotinimidamide were prepared according to the literature method.[32] 3-Acetoxy-18β*H*-glycyretinic acid (**3**) (purity ∼95%) was obtained by us as a result of acetic acid hydrolysis of the drug substance "Glycyram" (VFS 42-419-75, manufactured by JSC Chimpharm (Shymkent, Kazakhstan)) according to the previously published procedure.[44]

The target compound 30-nor-3β-hydroxy-11-oxo-20-(3′-(pyridin-3″-yl)-1′,2′,4′-oxadiazol-5′-yl)-18β*H*-olean-12-en (**2g**) was obtained from 3-acetoxy-18β*H*-glycyretinic acid (**3**) according to the literature method[38] with a total yield of 64%. Details of the synthetic path, physicochemical characteristics, and NMR spectral information on the target compound **2g** and its intermediates **1g** and **4g** are presented in Section S1 and Figures S3−S8.

The target compound 30-nor-3β-hydroxy-11-oxo-20-(3′-(4-florophenyl)-1′,2′,4′-oxadiazol-5′-yl)-18β*H*-olean-12-en (**2k**) was obtained from 3-acetoxy-18β*H*-glycyretinic acid (**3**) in a total yield of 55%. Details of the synthetic path, physicochemical characteristics, and NMR spectral information on the target compound **2k** and its intermediates **1k** and **4k** are presented in S1 and Figures S9−S14.

4.2. CELL CULTURES

Human cervical carcinoma KB-3-1 cells were purchased from the Russian Culture Collection (Institute of Cytology of the Russian Academy of Sciences, Saint Petersburg, Russia), and its subtype with MDR phenotype KB-8-5 cells were generously donated by Prof. M. Gottesman (National Institutes of Health, Bethesda, USA). Murine lymphosarcoma RLS cells were kindly provided by Prof. N.A. Popova (Institute of Cytology and Genetics, Siberian Branch of RAS, Novosibirsk, Russia) and its subtype with MDR phenotype RLS40 cells were purchased from the cell bank of the Institute of Chemical Biology and Fundamental Medicine SB RAS (Novosibirsk, Russia). The cells were grown in Dulbecco's modified Eagle's medium (DMEM) (Sigma-Aldrich, St. Louis, USA) (KB-3-1 and KB-8-5) and Iscove's Modified Dulbecco's Medium (IMDM) (Sigma-Aldrich, USA) (RLS and RLS40) containing 10% (v/v) heat-inactivated fetal bovine serum (FBS) (Gibco, UK), penicillin at 10 000 IU/mL, streptomycin at 10 000 μg/mL, and amphotericin at 25 μg/mL (MP Biomedicals, Illkirch-Graffenstaden, France). KB-8-5 and RLS40 cells were cultured in the presence of vinblastine at 300 or 40 nM, respectively. The cells were incubated at 37 °C in 5% CO_2 (hereafter, standard conditions). Triterpenoid derivatives were dissolved in DMSO at 10 mM (stock solution) and kept at −20 °C until further use.

4.3. MTT TEST

The KB-8-5 and KB-3-1 cells were seeded in quadruplicate at a density of 10^4 cells per well in 96-well plates with a final volume of 100 μL per well. After 24 h of incubation, the medium was replaced with a fresh medium (100 μL/well) containing different concentrations of triterpenoids (2.5, 5, 10, and 20 μM), GA (5 and 20 μM), or doxorubicin (1, 2, 5, and 10 μM). The cells were incubated in the presence or absence of the compounds (control) for an additional 72 h under standard conditions. Aliquots of MTT solution (10 μL, 5 mg/mL in PBS) (Sigma-Aldrich, USA) were then added to each well, followed by the incubation for an additional 2 h. After

https://doi.org/10.1021/acsomega.3c06202
ACS Omega 2023, 8, 48813−48824

incubation, the medium was replaced with DMSO to dissolve the formazan crystals, and the absorbance was determined at 570 and 620 nm in a Multiscan RC plate reader (Thermo LabSystems, Helsinki, Finland), followed by calculation of the cell viability rate in the experimental groups compared to the control.

4.4. WATER-SOLUBLE TETRAZOLIUM (WST) TEST

To determine the cytotoxicity of GA derivatives in RLS40 and RLS cells, a WST test was performed. The cells were seeded in quadruplicate at a density of 4×10^4 cells per well in 96-well plates with a final volume of 100 μL per well. After 24 h of incubation, the medium was replaced with fresh medium (100 μL/well) containing different concentrations of triterpenoids (2.5, 5, 10, and 20 μM). The cells were incubated in the presence or absence of compounds (control) for an additional 72 h under standard conditions. Following incubation with triterpenoids, 10 μL of WST-1 at 0.5 mg/mL (Roche, Switzerland) was added to each well. The cells were then incubated with WST-1 for 3 h under standard conditions. Thereafter, the absorbance was measured at the test and reference wavelengths (450 and 620 nm, respectively) using a Multiscan RC plate reader (Thermo LabSystems, Helsinki, Finland)), followed by calculation of the cell viability rate in the experimental groups compared to the control.

4.5. COMBINED CYTOTOXICITY OF 2G AND DOXORUBICIN

Cells were plated in a 96-well plate at 10^4 (KB-8-5) or 4×10^4 (RLS40) cells per well. After 24 h of incubation, the medium was replaced with a fresh medium containing diluted **2g** at various concentrations (2.5−20 μM) and DOX (2−32 μM) separately and in combination in quadruplicate, followed by the incubation of the cells for 72 h under standard conditions. Furthermore, the viability of the cells was assessed by using the MTT and WST assays mentioned above. The effect of the drug combination was determined by the Bliss model using the SynergyFinder software (https://synergyfinder.fimm.fi/).[40] The synergy score less than −10 indicates antagonism, a synergy score between −10 and 10 suggests an additive effect, and a synergy score greater than 10 indicates synergy.

4.6. RHODAMINE 123 ACCUMULATION ASSAY

For the Rhodamine 123 (Rho123) accumulation assay, the cells were plated in a 24-well plate at 10^5 cells/well for 24 h. The cells were then incubated in fresh medium containing Rho123 (5.25 μM) with or without (control) **2g** and **2k** (5 μM for KB-3-1 and KB-8-5 cells, 10 μM for RLS40 cells) or the known P-gp inhibitor verapamil (VPM; 50 μM), followed by incubation of the cells under standard conditions for 30 min. After being washed twice with ice-cold PBS and digested with the TrypLE Express (Gibco, Grand Island, NY, USA), the cells were collected, resuspended in fresh medium, and intracellular Rho123 fluorescence was measured with a NovoCyte Flow Cytometer (ACEA Biosciences, San Diego, USA). Ten thousand events were collected for each sample.

4.7. DOXORUBICIN ACCUMULATION ASSAY

For the DOX accumulation assay, the cells were plated in a 24-well plate at a density of 10^5 cells/well for 24 h. The medium was then changed to a fresh medium containing DOX (2 μM) (control), **2g** (5 μM for KB-8-5, 10 μM for RLS40), and VPM (50 μM), and the plate was incubated under standard conditions for 2 h. After being washed twice with ice-cold PBS and digested with the TrypLE Express (Gibco, Grand Island, NY, USA), the cells were collected and resuspended in fresh medium, and intracellular DOX fluorescence was measured with a NovoCyte Flow Cytometer (ACEA Biosciences, USA). Ten thousand events were collected for each sample.

4.8. ANALYSIS OF ABCB1 EXPRESSION BY REAL-TIME QUANTITATIVE POLYMERASE CHAIN REACTION (RT-QPCR)

Total RNA was isolated from cells using the TRIzol reagent (Ambion, Austin, USA) according to the manufacturer's protocol. The first cDNA strand was synthesized from total RNA in the reaction mixture (100 μL) containing 20 μL of 5× RT buffer (Biolabmix, Novosibirsk, Russia), 250 U of M-MuLV-RH-revertase (Biolabmix, Novosibirsk, Russia), 4 μg of total RNA, and 100 μM of the oligo (dT) primer. Reverse transcription was conducted at 42 °C for 60 min followed by a denaturation step at 70 °C for 10 min. Afterward, cDNA amplification was carried out using the following protocol: an initial denaturation step at 94 °C for 5 min with 40 subsequent 40 cycles of amplification (95 °C for 30 s, 59 °C for 30 s, and 72 °C for 30 s). The final reaction mixture for amplification (25 μL/probe) included 12.5 μL of HS-qPCR (2×) master mix (Biolabmix, Novosibirsk, Russia), 5 μL of cDNA, and 0.25 μM of forward and reverse primers (Table 1). The relative expression of genes was normalized to GAPDH and calculated by the ΔΔCt method using the CFX96 Real-Time system (Bio-Rad, Hercules, USA).

Table 1. Sequences of Primers for RT-PCR

gene	type	sequence
ABCB1	forward	5′- AATGGCTACATGAGAGCGGAG-3′
	reverse	5′-AATGTTCTGGCTTCCGTTGC-3′
GAPDH	forward	5′-ACCCCCAATGTGTCCGTCGT-3′
	reverse	5′-TACTCCTTGGAGGCCATGTA-3′

4.9. WESTERN BLOTTING

After **2g** treatment, KB-8-5 cells were lysed in the sample buffer (Sigma-Aldrich, St. Louis, Missouri, USA). Protein samples were separated by electrophoresis on SDS-PAGE gels and transferred to a polyvinylidene fluoride (PVDF) membrane (Millipore, USA), which were washed and blocked overnight in 2% nonfat dry milk in 0.05 M Tris-HCl, 0.15 M NaCl, and 0.1% Tween-20 (pH 7.5). The membranes were then incubated overnight with primary monoclonal antibodies P-glycoprotein (P7965, dilution 1:750, Sigma-Aldrich, St. Louis, USA) and GAPDH (A19056, dilution 1:5000, ABclonal, Wuhan, China), washed in 0.05 M Tris-HCl, 0.15 M NaCl, 0.1% Tween-20 (pH 7.5), and incubated with horseradish peroxidase-conjugated goat antimouse (A9917, dilution: 1:5000, Sigma-Aldrich, St. Louis, USA) or goat antirabbit (ab6721, dilution: 1:3000, Abcam, Waltham, USA) secondary antibodies for 1 h. Immunoreactive bands were detected with a Western Blotting Chemiluminescent Reagent Kit (Abcam, USA) using iBright Analysis Software v. 5.1.0 (Thermo Fisher Scientific, Waltham, USA) (Figure S2).

https://doi.org/10.1021/acsomega.3c06202
ACS Omega 2023, 8, 48813−48824

4.10. FLOW CYTOMETRY ANALYSIS OF P-GGP EXPRESSION

KB-8-5 cells were seeded on 24-well plates at 5×10^4 cells/well, and **2g** (5 μM) was added after 24 h. After 2 or 72 h, samples were processed for flow cytometry analysis. The growth medium was removed, and the cells were washed with PBS solution (MP Biomedicals, United States); then, the cells were trypsinized and transferred to 1.5 mL tubes. The cells were then pelleted by centrifugation at 400*g* for 5 min, the supernatant was removed, and the cells were incubated with mouse monoclonal anti-P-gp antibody (P7965, dilution 1:300, Sigma-Aldrich, St. Louis, USA) in PBS with 2% fetal bovine serum for 30 min at RT. The cells were washed with PBS and incubated with antimouse IgG conjugated with Alexa Fluor 488 (A21202, dilution: 1:200, Thermo Fisher Scientific, Waltham, USA) under the same conditions. After being washed, the cells were analyzed using a NovoCyte Flow Cytometer (ACEA Biosciences, USA). Fluorescence intensity was measured at a laser excitation wavelength of 488 nm, and emission was estimated by using an optical filter at 530 ± 30 nm. For each sample, 15 000 cells were analyzed; the expression level (%) was obtained by calculating the average fluorescence of treated cells minus control cells stained with Alexa Fluor 488-conjugated antibody only.

4.11. MOLECULAR DOCKING

The molecular docking of GA derivatives with P-gp was performed using AutoDock Vina.[45] The crystal structure of human ABCB1 complexed with zosuquidar (PDB ID: 7A6F) was retrieved from the RCSB PDB database and used as a docking template. All solvent molecules, water molecules, and zosuquidar were removed following the addition of polar hydrogens and Gasteiger charges using AutoDock Tools 1.5.7. The three-dimensional structures of ligands were created using Marvin Sketch 5.12, and their geometry was optimized using Avogadro 1.2.0 (MMFF94 force field). All rotatable bonds within the compound structures were allowed to be freely flexible. The grid box of 18 × 18 × 18, centered at [*x*, *y*, *z* = 161.718, 158.298, 159.204], was set to cover the entire zosuquidar binding pocket. Other parameters were set to their default values. The Discovery Studio Visualizer 17.2.0 (Dassault Systèmes, Cedex, France) was used to analyze the docking results.

4.12. *IN SILICO* PREDICTION OF P-GGLYCOPROTEIN (P-GGP) SUBSTRATE AND INHIBITOR SPECIFICITY OF INVESTIGATED COMPOUNDS

The potential of the investigated compounds to function as substrates or inhibitors of P-gp was assessed using ADMETlab (https://admet.scbdd.com/), SwissADME (http://www.swissadme.ch/), Vienna LiverTox Workspace (https://livertox.univie.ac.at/), and PreADMET (https://preadmet.qsarhub.com/adme/).

4.13. STATISTICAL ANALYSIS

Statistical analysis of mean differences between groups (n = 2 or 3 with 3−5 technical replicates) was performed by Student's t-test using Microsoft Excel (Microsoft, Redmond, USA), and $p < 0.05$ was considered as a statistically significant difference.

■ ASSOCIATED CONTENT

Supporting Information

The Supporting Information is available free of charge at https://pubs.acs.org/doi/10.1021/acsomega.3c06202.

Chemical experimental procedures; synthetic path and physicochemical characteristics of GA derivatives; figure demonstrating the toxic effect of **2g** against HEK293 cells; representative picture of Western blot analysis of P-glycoprotein levels in **2g**-treated KB-8-5 cells; spectral data of GA derivatives (^{1}H NMR and ^{13}C NMR) (PDF)

■ AUTHOR INFORMATION

Corresponding Author

Andrey V. Markov − *Institute of Chemical Biology and Fundamental Medicine Siberian Branch of the Russian Academy of Sciences, Novosibirsk 630090, Russia;* orcid.org/0000-0001-7569-9555; Email: andmrkv@gmail.com

Authors

Arseny D. Moralev − *Institute of Chemical Biology and Fundamental Medicine Siberian Branch of the Russian Academy of Sciences, Novosibirsk 630090, Russia; Faculty of Natural Sciences, Novosibirsk State University, Novosibirsk 630090, Russia;* orcid.org/0000-0001-7569-9555

Oksana V. Salomatina − *Institute of Chemical Biology and Fundamental Medicine Siberian Branch of the Russian Academy of Sciences, Novosibirsk 630090, Russia; N.N. Vorozhtsov Novosibirsk Institute of Organic Chemistry Siberian Branch of the Russian Academy of Sciences, Novosibirsk 630090, Russia*

Ivan V. Chernikov − *Institute of Chemical Biology and Fundamental Medicine Siberian Branch of the Russian Academy of Sciences, Novosibirsk 630090, Russia*

Nariman F. Salakhutdinov − *N.N. Vorozhtsov Novosibirsk Institute of Organic Chemistry Siberian Branch of the Russian Academy of Sciences, Novosibirsk 630090, Russia*

Marina A. Zenkova − *Institute of Chemical Biology and Fundamental Medicine Siberian Branch of the Russian Academy of Sciences, Novosibirsk 630090, Russia;* orcid.org/0000-0003-4044-1049

Complete contact information is available at: https://pubs.acs.org/10.1021/acsomega.3c06202

Funding

This research was supported by the Russian Science Foundation (Grant No. 23-14-00374) (synthesis, *in silico* and *in vitro* studies) and partly by the Russian state-funded budget project of ICBFM SB RAS No. 121031300044-5 (the use of the equipment).

Notes

The authors declare no competing financial interest.

■ ACKNOWLEDGMENTS

The authors gratefully thank Albina V. Vladimirova (Institute of Chemical Biology and Fundamental Medicine SB RAS, Novosibirsk, Russia) for cell maintenance and the Multi-Access Chemical Research Center SB RAS (Novosibirsk, Russia) for spectral and analytical measurements.

REFERENCES

(1) Bukowski, K.; Kciuk, M.; Kontek, R. Mechanisms of Multidrug Resistance in Cancer Chemotherapy. *Int. J. Mol. Sci.* **2020**, *21* (9), 3233.

(2) Amawi, H.; Sim, H.-M.; Tiwari, A. K.; Ambudkar, S. V.; Shukla, S.. ABC Transporter-Mediated Multidrug-Resistant Cancer. In *Drug Transporters in Drug Disposition, Effects and Toxicity*; Liu, X.; Pan, G., Eds.; Springer: Singapore, 2019; pp 549−580.

(3) Fletcher, J. I.; Williams, R. T.; Henderson, M. J.; Norris, M. D.; Haber, M. ABC Transporters as Mediators of Drug Resistance and Contributors to Cancer Cell Biology. *Drug Resistance Updates* **2016**, *26*, 1.

(4) Thomas, H.; Coley, H. M. Overcoming Multidrug Resistance in Cancer: An Update on the Clinical Strategy of Inhibiting P-Glycoprotein. *Cancer Control* **2003**, *10* (2), 159−165.

(5) Mealey, K. L.; Fidel, J. P-Glycoprotein Mediated Drug Interactions in Animals and Humans with Cancer. *J. Vet. Intern. Med.* **2015**, *29*, 1−6.

(6) Dong, J.; Qin, Z.; Zhang, W.-D.; Cheng, G.; Yehuda, A. G.; Ashby, C. R., Jr.; Chen, Z.-S.; Cheng, X.-D.; Qin, J.-J. Medicinal Chemistry Strategies to Discover P-Glycoprotein Inhibitors: An Update. *Drug Resistance Updates* **2020**, *49*, 100681.

(7) Zhang, H.; Xu, H.; Ashby, C. R., Jr.; Assaraf, Y. G.; Chen, Z.-S.; Liu, H.-M. Chemical Molecular-Based Approach to Overcome Multidrug Resistance in Cancer by Targeting P-Glycoprotein (P-Gp). *Med. Res. Rev.* **2021**, *41* (1), 525−555.

(8) Dong, J.; Yuan, L.; Hu, C.; Cheng, X.; Qin, J.-J. Strategies to Overcome Cancer Multidrug Resistance (MDR) through Targeting P-Glycoprotein (ABCB1): An Updated Review. *Pharmacol. Ther.* **2023**, *249*, 108488.

(9) Dewanjee, S.; Dua, T. K.; Bhattacharjee, N.; Das, A.; Gangopadhyay, M.; Khanra, R.; Joardar, S.; Riaz, M.; De Feo, V.; Zia-Ul-Haq, M. Natural Products as Alternative Choices for P-Glycoprotein (P-Gp) Inhibition. *Molecules* **2017**, *22* (6), 871.

(10) Abdallah, H. M.; Al-Abd, A. M.; El-Dine, R. S.; El-Halawany, A. M. P-Glycoprotein Inhibitors of Natural Origin as Potential Tumor Chemo-Sensitizers: A Review. *J. Adv. Res.* **2015**, *6* (1), 45−62.

(11) Kumar, A.; Jaitak, V. Natural Products as Multidrug Resistance Modulators in Cancer. *Eur. J. Med. Chem.* **2019**, *176*, 268−291.

(12) Gonçalves, B. M. F.; Cardoso, D. S. P.; Ferreira, M.-J. U. Overcoming Multidrug Resistance: Flavonoid and Terpenoid Nitrogen-Containing Derivatives as ABC Transporter Modulators. *Molecules* **2020**, *25* (15), 3364.

(13) Seelig, A.; Landwojtowicz, E. Structure-Activity Relationship of P-Glycoprotein Substrates and Modifiers. *Eur. J. Pharm. Sci.* **2000**, *12* (1), 31−40.

(14) Huang, W.; Wang, Y.; Xu, S.; Qiao, H.; Cheng, H.; Wang, L.; Liu, S.; Tian, Q.; Wang, R.; Wang, H.; Bi, Y. Design, Synthesis, and Tumor Drug Resistance Reversal Activity of Novel Hederagenin Derivatives Modified by Nitrogen-Containing Heterocycles. *Eur. J. Med. Chem.* **2022**, *232*, 114207.

(15) Yang, Y.; Guan, D.; Lei, L.; Lu, J.; Liu, J. Q.; Yang, G.; Yan, C.; Zhai, R.; Tian, J.; Bi, Y.; Fu, F.; Wang, H. H6, a Novel Hederagenin Derivative, Reverses Multidrug Resistance in Vitro and in Vivo. *Toxicol. Appl. Pharmacol.* **2018**, *341*, 98−105.

(16) Callies, O.; Sánchez-Cañete, M. P.; Gamarro, F.; Jiménez, I. A.; Castanys, S.; Bazzocchi, I. L. Optimization by Molecular Fine Tuning of Dihydro-β-Agarofuran Sesquiterpenoids as Reversers of P-Glycoprotein-Mediated Multidrug Resistance. *J. Med. Chem.* **2016**, *59* (5), 1880−1890.

(17) Yang, C.; Wong, I. L. K.; Peng, K.; Liu, Z.; Wang, P.; Jiang, T.; Jiang, T.; Chow, L. M. C.; Wan, S. B. Extending the Structure−activity Relationship Study of Marine Natural Ningalin B Analogues as P-Glycoprotein Inhibitors. *Eur. J. Med. Chem.* **2017**, *125*, 795−806.

(18) Rybalkina, E. Y.; Moiseeva, N. I.; Karamysheva, A. F.; Eroshenko, D. V.; Konysheva, A. V.; Nazarov, A. V.; Grishko, V. V. Triterpenoids with Modified A-Ring as Modulators of P-Gp-Dependent Drug-Resistance in Cancer Cells. *Chem.-Biol. Interact.* **2021**, *348*, 109645.

(19) Markov, A. V.; Odarenko, K. V.; Sen'kova, A. V.; Ilyina, A. A.; Zenkova, M. A. Evaluation of the Antitumor Potential of Soloxolone Tryptamide against Glioblastoma Multiforme Using in Silico, in Vitro, and in Vivo Approaches. *Biochemistry (Moscow)* **2023**, *88* (7), 1008−1021.

(20) Salomatina, O. V.; Sen'kova, A. V.; Moralev, A. D.; Savin, I. A.; Komarova, N. I.; Salakhutdinov, N. F.; Zenkova, M. A.; Markov, A. V. Novel Epoxides of Soloxolone Methyl: An Effect of the Formation of Oxirane Ring and Stereoisomerism on Cytotoxic Profile, Anti-Metastatic and Anti-Inflammatory Activities In Vitro and In Vivo. *Int. J. Mol. Sci.* **2022**, *23* (11), 6214.

(21) Ryu, K.; Susa, M.; Choy, E.; Yang, C.; Hornicek, F. J.; Mankin, H. J.; Duan, Z. Oleanane Triterpenoid CDDO-Me Induces Apoptosis in Multidrug Resistant Osteosarcoma Cells through Inhibition of Stat3 Pathway. *BMC Cancer* **2010**, *10* (1), 187.

(22) Laiolo, J.; Barbieri, C. L.; Joray, M. B.; Lanza, P. A.; Palacios, S. M.; Vera, D. M. A.; Carpinella, M. C. Plant Extracts and Betulin from Ligaria Cuneifolia Inhibit P-Glycoprotein Function in Leukemia Cells. *Food Chem. Toxicol.* **2021**, *147*, 111922.

(23) Zhang, C. Fluorine in Medicinal Chemistry: In Perspective to COVID-19. *ACS Omega* **2022**, *7* (22), 18206−18212.

(24) Dong, J.; Wang, N.-N.; Yao, Z.-J.; Zhang, L.; Cheng, Y.; Ouyang, D.; Lu, A.-P.; Cao, D.-S. ADMETlab: A Platform for Systematic ADMET Evaluation Based on a Comprehensively Collected ADMET Database. *J. Cheminform.* **2018**, *10* (1), 1−11.

(25) Daina, A.; Michielin, O.; Zoete, V. SwissADME: A Free Web Tool to Evaluate Pharmacokinetics, Drug-Likeness and Medicinal Chemistry Friendliness of Small Molecules. *Sci. Rep.* **2017**, *7*, 42717.

(26) Montanari, F.; Knasmüller, B.; Kohlbacher, S.; Hillisch, C.; Baierová, C.; Grandits, M.; Ecker, G. F. Vienna LiverTox Workspace—A Set of Machine Learning Models for Prediction of Interactions Profiles of Small Molecules With Transporters Relevant for Regulatory Agencies. *Front. Chem.* **2020**, *7*, 899.

(27) Mirzaei, S.; Gholami, M. H.; Hashemi, F.; Zabolian, A.; Farahani, M. V.; Hushmandi, K.; Zarrabi, A.; Goldman, A.; Ashrafizadeh, M.; Orive, G. Advances in Understanding the Role of P-Gp in Doxorubicin Resistance: Molecular Pathways, Therapeutic Strategies, and Prospects. *Drug Discovery Today* **2022**, *27* (2), 436−455.

(28) Chufan, E. E.; Kapoor, K.; Ambudkar, S. V. Drug−Protein Hydrogen Bonds Govern the Inhibition of the ATP Hydrolysis of the Multidrug Transporter P-Glycoprotein. *Biochem. Pharmacol.* **2016**, *101*, 40−53.

(29) Farman, S.; Javed, A.; Arshia; Khan, K. M.; Nasir, A.; Khan, A. U.; Lodhi, M. A.; Gul, H.; Khan, F.; Asad, M.; Parveen, Z. Benzophenone Sulfonamide Derivatives as Interacting Partners and Inhibitors of Human P-Glycoprotein. *Anti-Cancer Agents Med. Chem.* **2020**, *20* (14), 1739−1751.

(30) Singh, S.; Prasad, N. R.; Chufan, E. E.; Patel, B. A.; Wang, Y. J.; Chen, Z. S.; Ambudkar, S. V.; Talele, T. T. Design and Synthesis of Human ABCB1 (P-Glycoprotein) Inhibitors by Peptide Coupling of Diverse Chemical Scaffolds on Carboxyl and Amino Termini of (S)-Valine-Derived Thiazole Amino Acid. *J. Med. Chem.* **2014**, *57* (10), 4058−4072.

(31) Cheon, J. H.; Kim, K. S.; Yadav, D. K.; Kim, M.; Kim, H. S.; Yoon, S. The JAK2 Inhibitors CEP-33779 and NVP-BSK805 Have High P-Gp Inhibitory Activity and Sensitize Drug-Resistant Cancer Cells to Vincristine. *Biochem. Biophys. Res. Commun.* **2017**, *490* (4), 1176−1182.

(32) Lacbay, C. M.; Menni, M.; Bernatchez, J. A.; Götte, M.; Tsantrizos, Y. S. Pharmacophore Requirements for HIV-1 Reverse Transcriptase Inhibitors That Selectively "Freeze" the Pre-Translocated Complex during the Polymerization Catalytic Cycle. *Bioorg. Med. Chem.* **2018**, *26* (8), 1713−1726.

(33) Gladkikh, D. V.; Sen'kova, A. V.; Chernikov, I. V.; Kabilova, T. O.; Popova, N. A.; Nikolin, V. P.; Shmendel, E. V.; Maslov, M. A.; Vlassov, V. V.; Zenkova, M. A.; Chernolovskaya, E. L. Folate-Equipped Cationic Liposomes Deliver Anti-MDR1-siRNA to the

https://doi.org/10.1021/acsomega.3c06202
ACS Omega 2023, 8, 48813−48824

Tumor and Increase the Efficiency of Chemotherapy. *Pharmaceutics* **2021**, *13* (8), 1252.
(34) Lakra, D. S.; B, P.; N, D.; T, D.; G, K.; N, R. P. Chemosensitizing Potential of Andrographolide in P-Glycoprotein Overexpressing Multidrug-Resistant Cancer Cell Lines. *Nat. Prod. Res.* **2023**, 1−6.
(35) Jouan, E.; Le Vée, M.; Mayati, A.; Denizot, C.; Parmentier, Y.; Fardel, O. Evaluation of P-Glycoprotein Inhibitory Potential Using a Rhodamine 123 Accumulation Assay. *Pharmaceutics* **2016**, *8* (2), 12.
(36) Chufan, E. E.; Kapoor, K.; Sim, H.-M.; Singh, S.; Talele, T. T.; Durell, S. R.; Ambudkar, S. V. Multiple Transport-Active Binding Sites Are Available for a Single Substrate on Human P-Glycoprotein (ABCB1). *PLoS One* **2013**, *8* (12), No. e82463.
(37) Nosol, K.; Romane, K.; Irobalieva, R. N.; Alam, A.; Kowal, J.; Fujita, N.; Locher, K. P. Cryo-EM Structures Reveal Distinct Mechanisms of Inhibition of the Human Multidrug Transporter ABCB1. *Proc. Natl. Acad. Sci. U. S. A.* **2020**, *117* (42), 26245−26253.
(38) Markov, A. V.; Sen'kova, A. V.; Popadyuk, I. I.; Salomatina, O. V.; Logashenko, E. B.; Komarova, N. I.; Ilyina, A. A.; Salakhutdinov, N. F.; Zenkova, M. A. Novel 3′-Substituted-1′,2′,4′-Oxadiazole Derivatives of 18*β*h-Glycyrrhetinic Acid and Their O-Acylated Amidoximes: Synthesis and Evaluation of Antitumor and Anti-Inflammatory Potential in Vitro and in Vivo. *Int. J. Mol. Sci.* **2020**, *21* (10), 3511.
(39) González, M. L.; Mariano, D.; Laiolo, J.; Joray, M. B.; Maccioni, M.; Palacios, S. M.; Molina, G.; Lanza, P. A.; Gancedo, S.; Rumjanek, V.; Carpinella, M. C. Mechanism Underlying the Reversal of Drug Resistance in P-Glycoprotein-Expressing Leukemia Cells by Pinoresinol and the Study of a Derivative. *Front. Pharmacol.* **2017**, *8*, 205.
(40) Ianevski, A.; He, L.; Aittokallio, T.; Tang, J. SynergyFinder: A Web Application for Analyzing Drug Combination Dose-Response Matrix Data. *Bioinformatics* **2017**, *33* (15), 2413−2415.
(41) Weidner, L. D.; Fung, K. L.; Kannan, P.; Moen, J. K.; Kumar, J. S.; Mulder, J.; Innis, R. B.; Gottesman, M. M.; Hall, M. D. Tariquidar Is an Inhibitor and Not a Substrate of Human and Mouse P-Glycoprotein. *Drug Metab. Dispos.* **2016**, *44* (2), 275−282.
(42) Patutina, O. A.; Mironova, N. L.; Logashenko, E. B.; Popova, N. A.; Nikolin, V. P.; Vasil'ev, G. V.; Kaledin, V. I.; Zenkova, M. A.; Vlasov, V. V. Cyclophosphamide Metabolite Inducing Apoptosis in RLS Mouse Lymphosarcoma Cells Is a Substrate for P-Glycoprotein. *Bull. Exp. Biol. Med.* **2012**, *152* (3), 348−352.
(43) Cascorbi, I.. P-Glycoprotein: Tissue Distribution, Substrates, and Functional Consequences of Genetic Variations. In *Drug Transporters*; Fromm, M. F.; Kim, R. B., Eds.; Springer: Berlin, Heidelberg, 2011; pp 261−283. .
(44) Tolstikov, G. A.; Baltina, L. A.; Grankina, V. P.; Kondratenko, R. M.; Tolstikova, T. G.. *Licorice: Biodiversity, Chemistry, Medical Applications (In Russian)*; Academic Publishing House: Novosibirsk, Russia, 2007.
(45) Trott, O.; Olson, A. J. AutoDock Vina: Improving the Speed and Accuracy of Docking with a New Scoring Function, Efficient Optimization, and Multithreading. *J. Comput. Chem.* **2010**, *31* (2), 455−461.

https://doi.org/10.1021/acsomega.3c06202
ACS Omega 2023, 8, 48813−48824